



**HAL**  
open science

# Thermomechanical impact of underground coal gasification exploitation

Farid Laouafa

► **To cite this version:**

Farid Laouafa. Thermomechanical impact of underground coal gasification exploitation. 3. International Symposium on Mine Safety Science and Engineering (ISMS 2016), Aug 2016, Montreal, Canada. pp.170-175. ineris-01854255

**HAL Id: ineris-01854255**

**<https://ineris.hal.science/ineris-01854255>**

Submitted on 4 Sep 2018

**HAL** is a multi-disciplinary open access archive for the deposit and dissemination of scientific research documents, whether they are published or not. The documents may come from teaching and research institutions in France or abroad, or from public or private research centers.

L'archive ouverte pluridisciplinaire **HAL**, est destinée au dépôt et à la diffusion de documents scientifiques de niveau recherche, publiés ou non, émanant des établissements d'enseignement et de recherche français ou étrangers, des laboratoires publics ou privés.

# Thermomechanical impact of Underground Coal Gasification exploitation

Laouafa Farid

Institut National de l'Environnement Industriel et des Risques- INERIS, F-60550 Verneuil-en-Halate, France

## ABSTRACT

Underground mining by coal combustion (Underground Coal Gasification - UCG) raises questions regarding the mechanical behavior of the site and the stability of the overburdened rock layers. By studying the underground reactor, its inlet and outlet, the key roles played by mechanical damage and thermo-mechanical phenomena were confirmed. Deformation or collapse above the cavity may cause a collapse in the overlying layers or a subsidence at the surface level. These phenomena highly depend on the thermo-poro-mechanical behaviour of the surrounding rock (host rocks). The numerical results presented in this paper were derived from models based on different assumptions describing a raw geological background. Both 3D and 2D nonlinear finite element modelling was conducted based on two different approaches. Based on the analysis of the numerical results, we were able to highlight the main factors influencing the behaviour and mechanical stability of the overburden, and consequently the UCG process evolution.

KEYWORDS: Underground; coal; combustion; mining; thermomechanic; modelling

## 1. INTRODUCTION

Underground Coal Gasification (UCG) is a process in which coal is burnt in situ without an explicit extraction of the matter (Bell 2011; Bhutto et al. 2013; Shafirovich et al. 2009). The efficiency of the process depends on the combustion properties of coal rock and other thermodynamic features of the physical phenomenon (temperature, pressure, mass transport related variable) (Williams 1985; Speight 2013).

In terms of cavity shape and its time evolution, the UCG resembles the longwall mining method (Peng et al. 1982, 1984, 2007; Shabanimashcool, 2012).

The UCG process involves high temperatures of around 1000°C, which will affect the host rock, changing its mechanical properties. Based on different tests and research of mudstone specimens from coal seams, Luo et al. (2011) shows that high temperatures cause thermal expansion of mudstone, and that the expansion increases with temperature, producing expansive stress in the surrounding rock of underground gasifiers. Brittle cracks are the main type of deformation. The temperature dependency of rock behavior has been the subject of intense research (Bauer 1983; Deng'gina et al. 1994; Dwivedia et al. 2008; Fjaer et al. 1992; Ide et al. 2010; Somerton 1992; Wolf 2006).

The UCG process may also have other environmental impacts in terms of pollution of groundwater and surface subsidence. The groundwater may be affected by gas or others chemical species transported through the rock porous matrix, and the initial or induced cracks and micro-cracks. At the ground surface, soil subsidence is expected. The extent of subsidence is dependent on the location of

the coal seam, its thickness, and the mechanical properties of the overburden.

The purpose of our article is related to the thermo-mechanical effects induced by the UCG process.

In this framework we performed finite element analyses of a case study coal site that could be exploited by this method. The numerical results presented in this paper were derived from models based on different assumptions describing a raw geological background. Both 3D and 2D nonlinear finite element modelling was conducted based on two approaches. The first one assumed the rock media as a perfect thermo-elastoplastic continuum. In the second one, and in order to simulate explicitly large space scale crack propagation, a method based on finite element deactivation was developed, which is built on a finite element mesh refinement and uses two failure criteria.

On the basis of the analysis of the numerical results, we were able to highlight two main factors that influence the behavior and mechanical stability of overburden, and consequently the sustainability of the UCG process.

## 2. UCG PROCESS

In the case of UCG, the shape of the cavity (first factor) and its evolution with time can be strongly modified by the thermo-mechanical behaviour of the host rocks. The second factor is the presence of a heat source whose location and intensity evolve with time. The thermal properties of rocks depend strongly on their mineralogical composition, porosity ( $\phi$ ), saturation, etc (Fjaer et al. 1992). Table 1 below gives values of porosity ( $\phi$ ), thermal conductivity ( $\lambda$ ) and specific heat capacity ( $\rho$ )

$c_p$ ), where  $\rho$  is the material density. Somerton (1992) has shown that for different rock materials, the thermal properties are not constant but temperature dependent.

Table 1: Thermal properties of some materials (Jaeger et al. 2007).

Rock Type	$\phi$	$\alpha$ ( $1/^\circ\text{K}$ )	$\lambda$ ( $\text{W}/\text{m}^\circ\text{K}$ )	$\rho c_p$ ( $\text{J}/\text{m}^3^\circ\text{K}$ )
Berea sandstone (dry)	0.162	$1.5 \times 10^{-6}$	2.34	$1.76 \times 10^6$
Boom clay (wet)	0.450	$3.3 \times 10^{-6}$	1.70	$2.82 \times 10^6$
Granodiorite	—	$4.7 \times 10^{-5}$	2.70	$1.90 \times 10^6$
Halite Salt (wet)	0.001	$4.0 \times 10^{-5}$	6.62	$1.89 \times 10^6$
Water	—	$6.6 \times 10^{-5}$	0.60	$4.17 \times 10^6$
Kerosene	—	$3.2 \times 10^{-4}$	0.13	$1.67 \times 10^6$

In Figure 1, we describe the Underground Coal Gasification (UCG) process. The injection of air is performed by a vertical well, while syngas (synthetic gas) resulting from coal combustion is extracted by the other well. The coal seams are made to react underground with insufficient oxygen for complete combustion to create syngas. Air is usually used as an oxidant. The oxygen and water within the coal seam react with the coal to produce syngas, which is withdrawn through a production well.

Figure 1 depicts the so called CRIP (Controlled, Retractable Injection Point) method, in which the injection point is gradually withdrawn as coal is consumed. This specific UCG industrial process uses two parallel wells also called Knife-edge CRIP. In this case the distance between the two wells axes is taken to be 20 m. The thickness of the coal seam is equal to 17.3 m. It is assumed that the total width of the burning front is equal to 30 m.

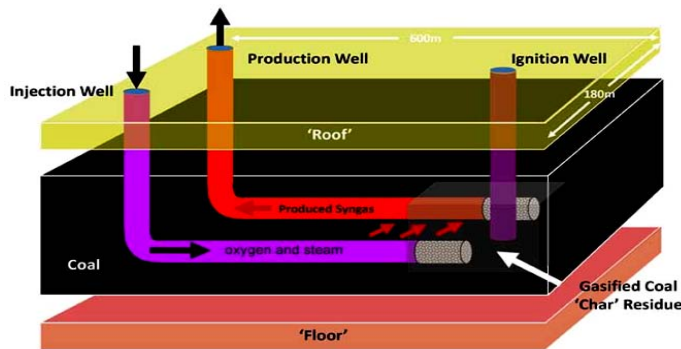


Figure 1: Schematic illustration of the adopted UCG industrial process with two wells.

The temperature at the combustion front is about  $1000^\circ\text{C}$  (after Total, a French multinational integrated oil and gas company). The burning front is assumed to be a straight plane at  $1000^\circ\text{C}$  and its normal velocity is about

$0.3\text{ mm}/\text{min}$  (after Total Company). The temperature within the cavity can reach several hundred degrees Celsius.

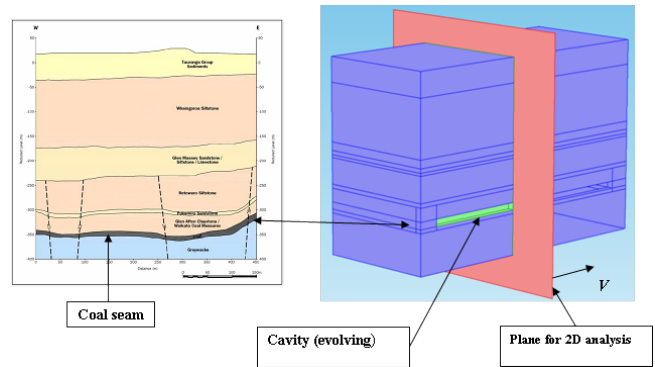


Figure 2: Stratigraphy and location of coal seam (on the left) and 3D numerical model (on the right). A 2D plane passing through the middle of exploitation used in plane strain numerical analyses.  $V$  stand for the burning front velocity.

In the case of a cavity (or gallery) having a geometric configuration such as that shown above, the deformation mechanism is mainly plane strain (plane perpendicular to the axis of the cavity). The plane strain analyses are based on a cavity width of 30 m. These dimensions assume that combustion extends 5 m transversely from two casings installed 20 m away from each other.

The reader can refer to Fjaer et al. (1992) for the mechanical and thermal properties of some of the rocks. Among all these properties that have been identified, some representative averaged values were extracted. The properties used in these models are as follows): Thermal conductivity:  $2\text{ W}/\text{m}/\text{K}$ , Heat capacity:  $800\text{ J}/\text{kg}/\text{K}$ , density:  $2500\text{ kg}/\text{m}^3$ .

The Young's Modulus of the coal is taken as  $2.5\text{ GPa}$  and Poisson's ratio as  $0.3$ . The Young's modulus of overburden is assumed to vary from  $5\text{ GPa}$  to  $25\text{ GPa}$  and the Poisson's ratio is equal to  $0.3$ . Several computations have been performed by varying these parameters within realistic value ranges, and they do not change our conclusions based on our modeling work. Low values for the Young's Modulus are assigned to the layers close to the surface in order to consider them as dead load. The thermal expansion coefficient of rocks is equal to  $10^{-5}\text{ }^\circ\text{C}^{-1}$ .

### 3. 2D AND 3D THERMOMECHANICAL MODELLING

The objective is to analyze the spatial extent of plasticity (damage) in the vicinity of the cavity. The model size is deliberately reduced to the dimensions defined in Figure 3. Although the model has a vertical plane of symmetry (through the axis of the cavity), the calculations were carried out on the whole 2D model to analyze a component of the robustness of the numerical

model (maintaining the symmetry of the mechanical response).

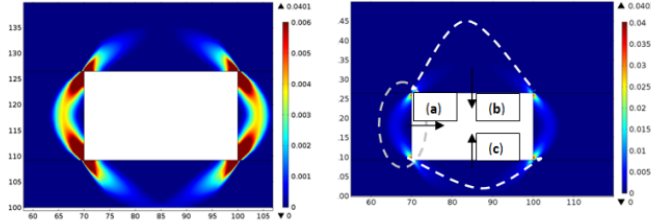


Figure 3: Spatial distribution of the effective plastic strain (in the left) and schematic of potential movements (failure, rockfalls, collapse,...) on the right.

Let us recall that the definition of the effective plastic strain is as follows:

$$\varepsilon_{eq}^p = \int_0^t \dot{\varepsilon}_{eq}^p dt \quad \text{with} \quad \dot{\varepsilon}_{eq}^p = \sqrt{\frac{2}{3} \dot{\varepsilon}_{ij}^p \dot{\varepsilon}_{ij}^p}$$

We observe that plasticity affects a part of the cover and the coal wall. However, the extension is limited but the coal layer is also affected.

We can assume that the hypotheses of material continuity and classical thermo-elastoplastic framework are too conservative. In other words, if the analysis was performed in the framework of fracture mechanics, linear or nonlinear (Broek 1986), we would certainly have found a lower overall stability rather than local rockfall from the roof and major collapse in coal (Figure 3, right). Likewise, it is reasonable to assume that overburden massive coal generally consists of calcareous clay layers, sometimes sandy, is layered, heterogeneous, and marked by discontinuities at different scales. The overall strength properties are quite low. Therefore, the choice of pair of values (cohesion, friction angle) representative of the whole overburden is critical for the prediction of the extent of the damaged area. We can a priori assume that the uniaxial compression strength of the overburden seldom exceeds 3 to 5 MPa overall. This leads to an extension of the damage larger than calculated above. These failure types can affect the combustion process as the combustion front may break and, due to the failures at the edge of the cavity, change the kinetics, the size, and shape of the combustion front, and therefore the shape of the cavity. They can also affect the direction of the cavity evolution. It is observed that the greatest displacement naturally lies in the cavity roof. The effect on the surface (subsidence) will be presented in the section dedicated to 3D models. If it is not explicitly specified, the criterion for the *adaptive mesh refinement* is based upon the value of the equivalent plastic strain.

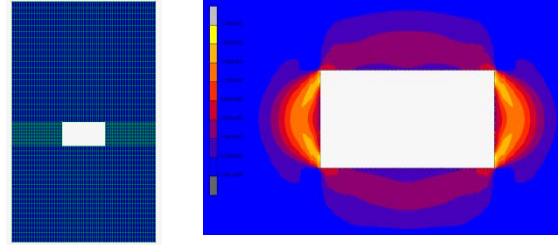


Figure 4: 2D finite elements mesh (left) and effective plastic strain (right) (L=30 m).

The model on which we performed our analysis is illustrated by its finite element mesh in Figure 4. The width of the cavity is 30 m. This approach required the use of another finite element code that allows adaptive mesh refinement and the possibility of deactivating a number of elements (MARC<sup>TM</sup> finite elements code, MSC Software, 2014). Figure 4 shows also spatial distribution of plasticity and Figure 5 presents the mesh density when using finite element refinement and deactivation in order to simulate crack propagation.

It was observed that the extension of the plasticity zone for a cavity of 30 m width is limited in space but still significant.

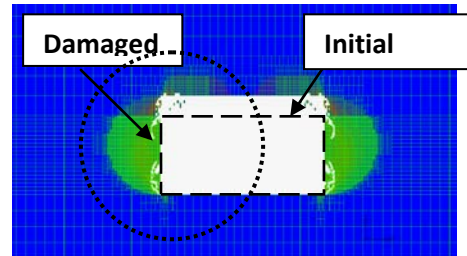


Figure 5: Example of result with adaptive mesh refinement and element deactivation (L = 30 m). The effective plastic deformation range from 0 to 0.17.

The results in Figure 4 are obtained through a classical approach and the elastoplastic continuum medium (i.e., overburden and coal) is assumed to be continuous and remains so regardless of the degree of "damage". Figures 5, 6, and 7 show the same computation, but using a deactivation (roughly simulating fracturing) of finite elements based on adaptive mesh refinement. We observe that with the most intense element concentration (small elements and therefore finer mesh), the damage zone becomes more detailed. Note also that the computation highlight the "failure" in the walls of the cavity and the collapse of part of the roof of the cavity.

On the basis of the spatial distribution of the mesh, it is easy to foresee the shape and damaged areas. The extent of mesh refinement is limited only by the power of the computer. The refinement is an *h-refinement* (based on subdivision of the finite element), which is different than *p-refinement* (based on the degree of the finite element).

The effect of the fineness of the mesh is shown in Figures 6 and 7.

The rock properties (reduction of cohesion and friction angle by 40%) were decreased and the cavity was widened to 30 m. The initial mesh was regular and relatively coarse (in size).

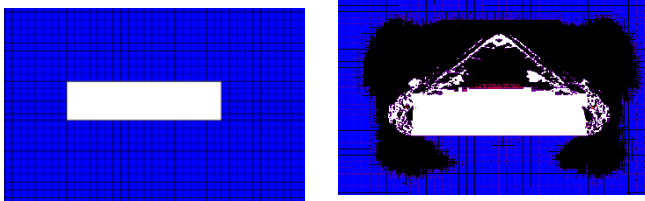


Figure 6: Initial mesh (left) and after dynamic computation, using adaptive mesh refinement and finite element deactivation (right). (Cavity width=30 m).

Figure 6 shows the distribution of fracturing in the overburden, in the coal walls, and the mesh density in the plasticity zones. Figure 7 (right) shows a focus of quality of mesh refinement required in order to carry out the calculation. The "triangular" shape of the collapse area in the roof and high degradation of coal wall are to be noted. This failure mode, described here in a very simplified way, is commonly observed in situ in the case of underground mines or quarries. The figures represent results at an instantaneous state (observation at a given time  $t$ ) because the elements are allowed to move in the dynamic analysis. The inertial terms induced by gravity and the fractures play an important role and this analysis therefore differs fundamentally from the quasi-static approach. The cavity extends laterally until the coal zone is sufficiently undamaged (by failure). The combustion process which is already a chaotic phenomenon would be difficult to formalize in such condition. The combination of burning and fracturing/block falling should influence the rate of combustion in the cavity.

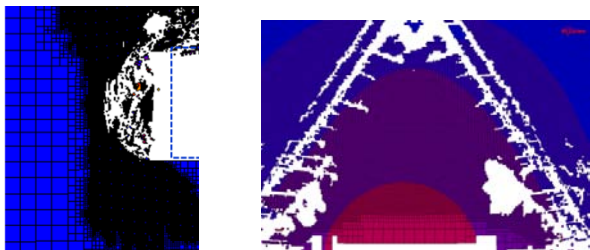


Figure 7: Focus of the coal wall and roof meshes (several thousand elements).

The modelling results depicted in Figures 6 and 7 present the main failure mechanisms as described by Whittles et al. (2007). The coal wall, the roof, and part of the floor are damaged by the cavity creation. This numerical computation using adaptive mesh refinement and element deactivation seems relevant for this study as they contain much information performed even on an idealized geometry such as failure and damage of the roof

and wall being important outcomes. It should be noted that such mechanisms are those generally observed during underground mining. In the case of UCG, these failures can disrupt the function of the reactor, alter the path of the combustion front, and so on.

#### 4. SUBSIDENCE AND ROOF DEFORMATION

The 3D computations are performed on the geometric model shown in Figure 8. The cavity and its spatio-temporal evolution are not explicitly created. More precisely, the initial cavity, a purely geometrical shape, has the dimensions of the final "cavity". However, it applies to the boundaries of the cavity pressure and temperature whose laws of spatial and temporal evolution describe the expansion of the cavity.

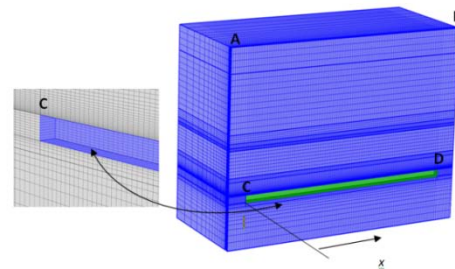


Figure 8: 3D mesh and location of the coal seam.

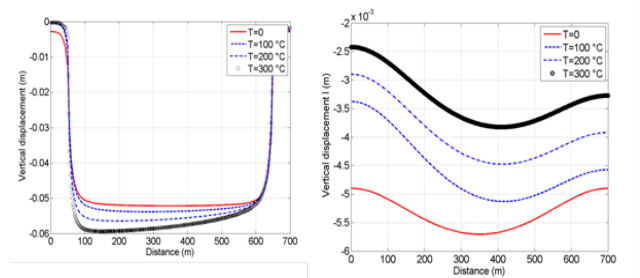


Figure 9: Vertical displacement of the roof of the cavity (segment CD) when it is created (left) and surface subsidence (segment AB) when the whole cavity is created (right) for 4 temperatures fields inside the cavity.

The first remark concerns the vertical displacement of the roof of the cavity. Asymmetry (with respect to the reference solution  $T=0$ ) occurs. Note in the modelling the "front" of combustion moves from left to right. The higher the temperature, the greater the intensity of movement (left increases), and the asymmetry is more pronounced. This is explained by the fact that by conduction and due to the intensity of the temperature difference, the part to the left is longer subjected to a high temperature. Consequently the extension of the temperature will be greater in the rock matrix. There is also a shift to the right for the maximum subsidence. The surface subsidence is induced not only by the excavation of the cavity, but also by thermal effects. That the subsidence is negative

indicates that the contribution of the rock mass thermal expansion in the uprising is lower than the displacement induced by stress modification due to underground excavation. The following 3D results are given as an illustration and show the burning front evolution. Elastoplastic models with adaptive refinement and 3D finite element deactivation were performed in order to assess the consequences of a possible "fracturing".

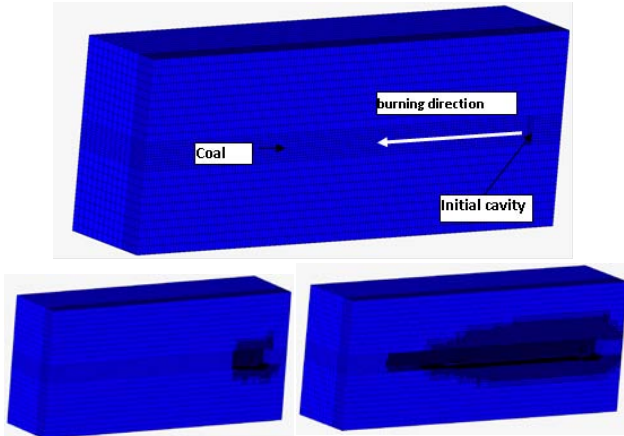


Figure 10: Example of induced "fracturing" during time and the space evolution of the cavity.

## 5. STRATIFIED ROOF

In this short subsection we analyze briefly the behavior of a stratified roof composed of marl and sandstone (Figure 11). The elliptical cavity is located in the coal layer. The remaining rock is sandstones.

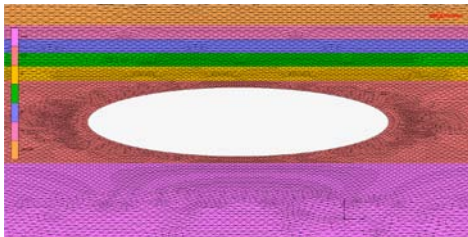


Figure 11: Mesh of the elliptical burning cavity and stratified roof.

After a given extend of the burning cavity (assumed elliptical in this sub-section), we applied a given temperature to its boundary (200 °C). After a given time we obtained the following displacement field as illustrated in Figure 12.

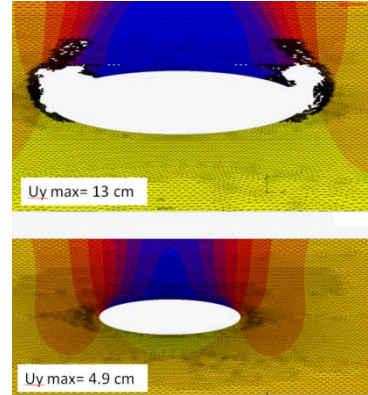


Figure 12: Vertical displacements field using two methods: Pseudo fracturing (top) and continuum model (bottom).

One can observe that the intensity of the vertical displacement and the final shape is strongly dependent on the assumption of a perfect continuum. The effect of the presence of layers with different mechanical parameters is show in Figure 13.

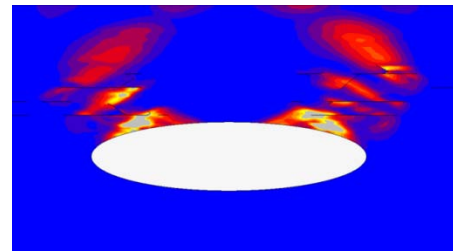


Figure 13: Effective plastic strain distribution with crack propagation.

The spatial distribution of the effective plastic strain is totally different when we take into account a layered roof. In this configuration that exhibits a stratified roof we highlight the transient effect of temperature. Indeed, thermal effects are more important when the medium is stratified and thus heterogeneous. The differential thermal and/or mechanical properties induce incremental strains and shear at interfaces layers. The case presented here is an academic and theoretical case. In real environments, we encounter heterogeneities at the porous matrix level, where it is well known and demonstrated that they induce an increase of the Von Mises stress. In addition, the results for a stratified medium show that solving such problems by using continuous media assumptions is far too conservative.

## 6. CONCLUSIONS

Geomechanical evaluations of the rock mass properties remain very important processes during Underground Coal Gasification. An accurate stability analysis of the consequence of UCG requires a global characterization of the rock constituting the overburden. All of the different factors contribute to instability of the

host rock during and after the gasification process. Unlike the stresses induced by void creation and their redistribution (as encountered in conventional mining), UCG introduced additional thermal stresses in the vicinity of the reactor. Thermal expansion may induce buckling or elastoplastic instability due to the increase of compressive stresses. The problem, which can be defined as transient bifurcation, is quite complex. The shape of the cavity and its evolution in time remain an important parameter which influences the stability of the host rock. Nevertheless, the evolution of the cavity in space and time has some random character due to the non-control of the parameters driving the combustion process and also due to the effects of host rock behavior. Caution must be taken when using a specific technique for UCG simulation.

## 7. ACKNOWLEDGEMENT

The work performed in this paper is supported by the EU project COGAR, Grant Agreement RFCR-CT-2013-00002.

## 8. REFERENCES

- Bell D.A., Towler B.F., Fan M. (2011). *Coal Gasification And Its Applications*. Elsevier
- Bhutto A.W., Bazmi A.A., Zahedi G. (2013). *Underground Coal Gasification: From fundamentals to applications*. *Progress in Energy and Combustion Science* 39, pp. 189-214
- Broek D. (1986). *Elementary Engineering Fracture Mechanics*, 4th ed., Kluwer, Dordrecht
- Den'gina N.I., Kazak V.N., Pristash (1994). *Changes in rocks at high temperatures. Geotechnological methods*. Plenum Publishing Corporation, pp. 472-777.
- Dwivedia R.D., Goela R. K., Prasada V.V.R., Sinhab (2008). Thermo-mechanical properties of Indian and other granites. *International Journal of Rock Mechanics & Mining Sciences*. 45, pp. 303–315
- Fjaer E, Holt R M, Horsrud P, Raaen A M , Risnes R (1992) *Petroleum related rock mechanics*. Elsevier
- Ide T.S., Pollard D, Orr F M (2010) Fissure formation and subsurface subsidence in a coalbed fire. *International Journal of Rock Mechanics and Mining Sciences*. Vol.7: 81–93
- Jaeger J.C., Cook N.G.W., Zimmerman R.W. (2007). *Fundamentals of Rock Mechanics*. Fourth Edition. Blackwell
- Luo J., Wang L. (2011). High-Temperature Mechanical Properties of Mudstone in the Process of Underground Coal Gasification. *Rock Mech Rock Eng* 44:749–754
- Marc Software (2014). *Marc user manual*.
- Peng S.S., Chiang H. S. (1982) Roof Stability in longwall coal face. in *Stability in Underground Mining*, Brawner C O ed. American Institut of mining, Metallurgical and petroleum Engineers, Inc.
- Peng S.S., Chiang H.S. (1984) *Longwall Mining*. Wiley
- Peng S.S., Zhang J. (2007). *Engineering Geology for Underground Rocks*. Springer-Verlag, Berlin Heidelberg.
- Shafirovich E., Varma A. (2009). *Underground Coal Gasification: A Brief Review of Current Status*. *Ind. Eng. Chem. Res.* 4 : 7865–7875
- Somerton W. H. (1992). *Thermal properties and temperature-related behavior of rock/fluid systems*. Elsevier.
- Speight J.G. (2013). *The Chemistry and Technology of Coal*. Third Edition. CRC Press
- Williams F. A. (1985). *Combustion Theory The Fundamental Theory of Chemically Reacting Flow Systems* Second Edition. Princeton University
- Wolf K. H. A. A.(2006). *The Interaction between Coal Fires and Their Roof Rocks*. Phd thesis, Delft University of Technology